BIOCHEMISTRY
including biophysical chemistry & molecular biology
Article

Biochemistry **2009,** *48,* 6175–6183 6175
DOI: 10.1021/bi900483b

Crystal Structure of (+)-δ-Cadinene Synthase from *Gossypium arboreum* and Evolutionary Divergence of Metal Binding Motifs for Catalysis[†,‡]

Heather A. Gennadios,[§] Veronica Gonzalez,[∥,#] Luigi Di Costanzo,[§,#,⊥] Amang Li,[∥] Fanglei Yu,[∥,@] David J. Miller,[∥] Rudolf K. Allemann,*[,∥] and David W. Christianson*[,§]

[§]*Roy and Diana Vagelos Laboratories, Department of Chemistry, University of Pennsylvania, Philadelphia, Pennsylvania 19104-6323,* [∥]*School of Chemistry, Cardiff University, Park Place, Cardiff CF10 3AT, United Kingdom,* [⊥]*Ben May Institute for Cancer Research, University of Chicago, Chicago, Illinois 60637, and* [@]*NewChem Technologies Ltd., Bedson Building, Kings Road, Newcastle upon Tyne NE1 7RU, United Kingdom* [#]*These authors made equal contributions to this study*

Received March 20, 2009; Revised Manuscript Received May 12, 2009

ABSTRACT: (+)-δ-Cadinene synthase (DCS) from *Gossypium arboreum* (tree cotton) is a sesquiterpene cyclase that catalyzes the cyclization of farnesyl diphosphate in the first committed step of the biosynthesis of gossypol, a phytoalexin that defends the plant from bacterial and fungal pathogens. Here, we report the X-ray crystal structure of unliganded DCS at 2.4 Å resolution and the structure of its complex with three putative Mg^{2+} ions and the substrate analogue inhibitor 2-fluorofarnesyl diphosphate (2F-FPP) at 2.75 Å resolution. These structures illuminate unusual features that accommodate the trinuclear metal cluster required for substrate binding and catalysis. Like other terpenoid cyclases, DCS contains a characteristic aspartate-rich $D^{307}DTYD^{311}$ motif on helix D that interacts with $Mg^{2+}{}_A$ and $Mg^{2+}{}_C$. However, DCS appears to be unique among terpenoid cyclases in that it does not contain the "NSE/DTE" motif on helix H that specifically chelates $Mg^{2+}{}_B$, which is usually found as the signature sequence (**N**,**D**)D(L,I,V)X(**S**,**T**)XXX**E** (boldface indicates $Mg^{2+}{}_B$ ligands). Instead, DCS contains a second aspartate-rich motif, $D^{451}DVAE^{455}$, that interacts with $Mg^{2+}{}_B$. In this regard, DCS is more similar to the isoprenoid chain elongation enzyme farnesyl diphosphate synthase, which also contains two aspartate-rich motifs, rather than the greater family of terpenoid cyclases. Nevertheless, the structure of the DCS−2F-FPP complex shows that the structure of the trinuclear magnesium cluster is generally similar to that of other terpenoid cyclases despite the alternative $Mg^{2+}{}_B$ binding motif. Analyses of DCS mutants with alanine substitutions in the $D^{307}DTYD^{311}$ and $D^{451}DVAE^{455}$ segments reveal the contributions of these segments to catalysis.

Antimicrobial natural terpenoid products known as phytoalexins are generated by tree cotton (*Gossypium arboreum*, indigenous to India and Pakistan) in response to threats from bacterial or fungal pathogens (*1*, *2*). These products are classified as secondary metabolites and are therefore nonessential for plant viability; however, they mediate important interactions between plants and their environments (*3*). The 64 kDa sesquiterpenoid cyclase (+)-δ-cadinene synthase (DCS,[1] isozyme XC1; SWISS-PROT accession code Q39761) catalyzes the formation of (+)-δ-cadinene from farnesyl diphosphate (FPP), which is the first committed step in the biosynthesis of the triterpene phytoalexin gossypol (*4*−*7*) (Figure 1). Gossypol is the predominant terpenoid found in the glands of aerial tissues and in epidermal cells of roots and is the major defense metabolite generated in cotton plants. Notably, gossypol has also been studied as a male contraceptive drug (*8*, *9*) and as a potential cancer chemotherapeutic agent (*10*−*13*).

The catalytic mechanism of DCS (Figure 1) is believed to be initiated by the metal-dependent isomerization of FPP to yield 3(*R*)-nerolidyl diphosphate (NPP), which then undergoes metal-dependent reionization after achieving a cisoid conformation to yield an allylic cation−pyrophosphate anion pair. The first carbon−carbon bond forming reaction in the cyclization cascade is electrophilic attack of C1 at the C10−C11 π-bond, which is followed by a 1,3-hydride shift from C2 to C11 to form the 3(*Z*),7(*E*)-germacryl cation. Subsequent electrophilic attack of the allylic C2 carbocation at the C7−C8 π-bond generates the cadinyl cation, which is ultimately quenched by deprotonation

[†]This work was supported by National Institutes of Health Grant GM56838 (D.W.C.), BBSRC Grants 6/B17177 (R.K.A.) and BB/G003572/1 (R.K.A.), EPSRC Grant EP/D06958/1 (R.K.A.), Royal Society Grant 2007R2 (R.K.A.), and Cardiff University.

[‡]The atomic coordinates of unliganded (+)-δ-cadinene synthase and its complex with 2-fluorofarnesyl diphosphate have been deposited in the Protein Data Bank as entries 3G4D and 3G4F, respectively.

*To whom correspondence should be addressed. D.W.C.: telephone: (215) 898-5714; fax: (215) 573-2201; e-mail: chris@sas.upenn.edu. R.K.A.: telephone: +44 29 2087 9014; fax: +44 29 2087 4030; e-mail: allemannrk@cardiff.ac.uk.

[1]Abbreviations: APS, Advanced Photon Source; ATAS, *Aspergillus terreus* aristolochene synthase; BME, β-mercaptoethanol; DCS, (+)-δ-cadinene synthase; FPP, farnesyl diphosphate; 2F-FPP, 2-fluorofarnesyl diphosphate; 10F-FPP, 10-fluorofarnesyl diphosphate; FPPS, farnesyl diphosphate synthase; GC−MS, gas chromatography−mass spectrometry; NPP, nerolidyl diphosphate; PEG, polyethylene glycol.

Published on Web 06/02/2009

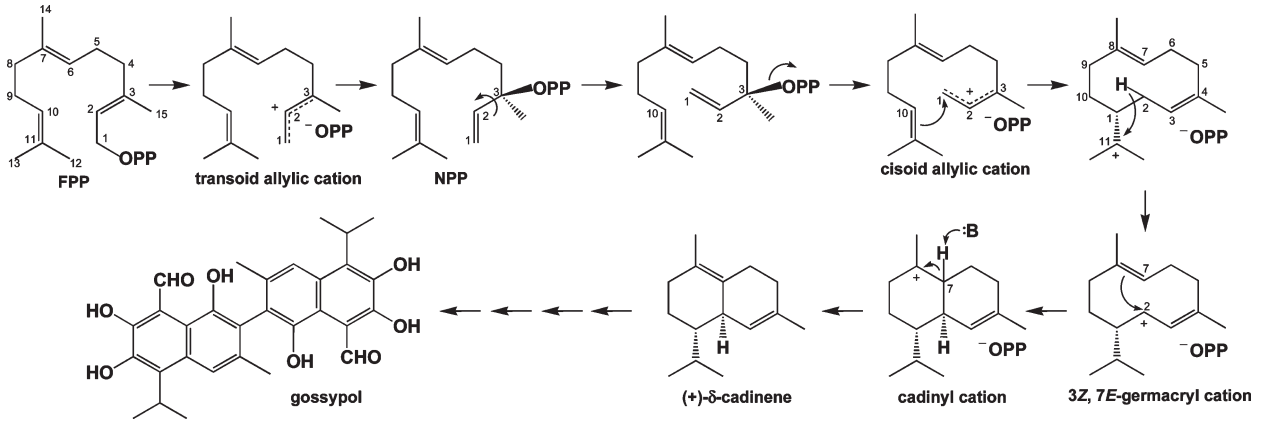

FIGURE 1: Proposed catalytic mechanism for (+)-δ-cadinene synthase from *G. arboreum* (*15*). The reaction is initiated by ionization and isomerization of farnesyl diphosphate (FPP) to yield nerolidyl diphosphate (NPP), which undergoes rotation about the C2−C3 bond and reionization to yield a cisoid allylic cation. Cyclization is achieved by formation of the C1−C10 bond, which is followed by a 1,3-hydride shift from C2 to C11 to form the 3(*Z*),7(*E*)-germacryl cation. Subsequent C7−C2 bond formation yields the cadinyl cation, which undergoes proton abstraction at C7 to generate (+)-δ-cadinene. While the identity of the base (B:) in the final step is not known, it is possible that the pyrophosphate leaving group ($^{-}$OPP, which represents $PO_4PO_3^{4-}$) serves this function, as proposed in the mechanisms of aristolochene synthase (*43*, *51*) and farnesyl diphosphate synthase (*22*). Further oxidation and coupling steps yield gossypol.

at C7 to form (+)-δ-cadinene (*5*, *14*, *15*). Recent gas-phase quantum chemical calculations support the viability of the postulated mechanism for the formation of the bicyclic cadinyl skeleton (*16*). Significantly, DCS is a "high-fidelity" terpenoid cyclase since it generates (+)-δ-cadinene nearly exclusively (>98%) (see the Supporting Information) (*15*). This contrasts with the output of more promiscuous cyclases such as γ-humulene synthase, which generates a total of 52 sesquiterpenoid products from substrate FPP (*17*).

On the basis of sequence alignments with other terpenoid cyclases, the amino acid sequence of DCS (*5*) indicates that helix D of the catalytic domain contains the aspartate-rich segment D^{307}DTYD^{311}, which is the signature **DD**XX(X)**D/E** metal binding motif common to terpenoid cyclases (boldface residues typically coordinate to Mg^{2+} ions). However, DCS does not contain the characteristic "NSE/DTE" metal binding motif on helix H, which is usually found as the signature (**N**,**D**)D(L,I,V)X-(**S**,**T**)XXX**E** sequence that specifically chelates $Mg^{2+}{}_B$ (*18*, *19*) [boldface indicates $Mg^{2+}{}_B$ ligands; occasionally, glycine is observed in place of (**S**,**T**), in which case an additional water molecule may coordinate to $Mg^{2+}{}_B$ (*20*)]. Instead, DCS contains a second aspartate-rich motif, D^{451}DVAE^{455}. Ordinarily, the NSE/DTE motif distinguishes a terpenoid cyclase from a terpenoid synthase that catalyzes an isoprenoid chain elongation reaction, such as farnesyl diphosphate synthase (*21*−*23*). Thus, the metal coordination polyhedra required for substrate binding and catalysis distinguish DCS from other terpenoid cyclases (*24*−*27*).

We recently reported the crystal structures of aristolochene synthase from *Aspergillus terreus* complexed with various fluorinated farnesyl diphosphate analogues (*28*). These structures reveal conformational changes that the enzyme can undergo upon complexation with substrate analogues and metal ions, thereby exemplifying the utility of fluorinated isoprenoid derivatives in the study of structure−function relationships. Here, we report the X-ray crystal structure of DCS from *G. arboreum* and the structure of its complex with 2-fluorofarnesyl diphosphate (2F-FPP). Additionally, we present product distribution and kinetic data for DCS mutants with aspartate → alanine and glutamate → alanine substitutions in the D^{307}DTYD^{311} and D^{451}DVAE^{455} segments. These results taken together illuminate aspects of metal binding in an unusual terpenoid cyclase active site and provide inferences regarding conformational changes that may occur upon substrate binding and catalysis.

MATERIALS AND METHODS

Synthesis of Fluorinated FPP Analogues. The substrate analogue 2F-FPP was prepared from geranyl acetone as previously described (*29*). The synthesis of 10F-FPP is outlined in the Supporting Information.

Expression and Purification. Plasmid pXC1 (a kind gift from X.-Y. Chen) containing the cDNA for DCS (*5*) was modified to introduce NcoI and BamHI sites at the 5′- and 3′-ends, respectively, using the primers 5′-CATGCCATGGCTTCACAAGTTTCTCAAATGCC-3′ and 5′-CGGGATCCTCAAAGTGCAATTGGTTCAATGAGC-3′ and then inserted into pET 21d (Stratagene). Rosetta2(DE3)pLysS cells were then transformed with this plasmid. Six single colonies of transformed cells were added to 5 mL of YT medium containing 50 μg/mL ampicillin and 34 μg/mL chloramphenicol. Cultures were grown overnight at 37 °C with shaking. The 5 mL overnight cultures were used to inoculate 6 × 500 mL of sterile YT medium containing the appropriate antibiotics. Cells were incubated at 37 °C with shaking until the absorbance at 600 nm was between 0.5 and 0.8. Expression was induced with 500 μM IPTG and the mixture incubated at 37 °C with shaking for 3 h. The cells were pelleted by centrifugation for 10 min at 6000 rpm, and the supernatant was decanted and discarded. The cell pellet was stored at −20 °C until it was needed.

Pellets were thawed and resuspended in 25 mL of cell lysis buffer [20 mM Tris (pH 8.0), 5 mM EDTA, and 5 mM β-mercaptoethanol (BME)]. Cells were lysed by sonication (50% duty cycle, 50% output) using 3 × 2 min pulses. The lysed cells were centrifuged at 16000 rpm for 30 min, and the supernatant was discarded (DCS remained solely in the insoluble portion). The pellets were resuspended in 150 mL of fresh lysis buffer and titrated on ice with light stirring with 0.1 M NaOH until the solution became clear (pH ~11.6). The solution was stirred on ice for 30 min. The pH was then lowered to pH 7.5 with 0.1 M HCl and BME added to a final concentration of 5 mM. The resulting solution was stirred on ice for 30 min and centrifuged at 16000 rpm. DCS remained in the soluble supernatant.

A 5 mL HiTrap DEAE Fast Flow column (GE Biosciences) was utilized. The column was washed with 5−10 column volumes of lysis buffer. The protein was loaded onto the column and washed with an additional 5−10 column volumes of lysis buffer. A linear gradient ranging from 0 to 600 mM NaCl was applied to the column and the protein eluted with ~240 mM NaCl. Fractions containing protein were analyzed on an SDS−PAGE gel and pooled together. The protein was concentrated to a total volume of ~6 mL. A 26/60 Superdex 200 size exclusion column (GE Biosciences) was washed with 1 column volume of buffer [20 mM Tris (pH 8.0), 50 mM NaCl, and 5 mM BME]. The protein eluted in two different peaks. The first peak eluted at the void volume for the column, indicating that the protein in this peak was most likely composed of soluble aggregates. The second peak corresponded to the molecular mass of the DCS monomer (64 kDa). The fractions were analyzed by SDS−PAGE, and those corresponding to the DCS monomer from the size exclusion chromatogram were pooled and concentrated to a final protein concentration of ~10 mg/mL. The estimated purity was >85%.

Site-directed mutagenesis of recombinant DCS cDNA is described in the Supporting Information. The expression and purification of mutant DCS enzymes was identical to that described above for wild-type DCS except that instead of using size exclusion chromatography in the final step, the protein was purified using a Resource Q column (GE Healthcare, 6 mL) eluting with a NaCl gradient from 0 to 1 M over 15 column volumes with enzymes eluting between 200 and 500 mM NaCl.

Steady-state kinetic parameters of the mutants were measured at 25 °C using a radiochemical assay modified slightly from that used to determine kinetic parameters for the sesquiterpene cyclase aristolochene synthase (*30*). Assays (final volume of 250 μL) were initiated by addition of a purified DCS solution (0.5 μM) to 1−200 μM [1-^{3}H]farnesyl diphosphate (240000 dpm/nmol) in 25 mM HEPES, 15 mM $MgCl_2$, and 5 mM DTT (pH 7.5). After incubation for 12 or 15 min, reactions were stopped by addition of 100 mM EDTA and overlaid with hexane (1 mL). After the samples had been vortexed for 10 s, the hexane was removed and the sample extracted with hexane in the same way (2 × 1 mL). The pooled fractions were passed through a short column containing approximately 500 mg of silica into a scintillation vial containing 15 mL of Ecoscint and analyzed by scintillation counting.

Inhibition assays were performed in identical fashion except for the addition of 2F-FPP at concentrations ranging from 0 to 120 μM. The IC_{50} value was calculated from inhibition assays at 8 μM FPP fitting the data (corrected using negative controls) to the equation $V_i/V_0 = 1/(1 + [I]/IC_{50})$, and the values for K_M and k_{cat} were calculated by fitting the data to the equation $v_5 = (k_{cat}[E_{total}][S])/(K_M + [S])$ using Systat Sigmaplot 10.

Incubation of DCS with FPP. The DCS solution (25 μL, 70 μM) was diluted with 500 μL of buffer consisting of 25 mM HEPES, 5 mM DTT, and 15 mM $MgCl_2$ (pH 7.5). The assay solution was gently mixed as 10 mM FPP (25 μL) was added followed by pentane (100 μL). After incubation for 24 h at 25 °C, the olefin products were extracted with pentane (3 × 1 mL). This solution was passed through a short pad of silica gel (~500 mg) and analyzed by gas chromatography−mass spectrometry (GC−MS). The GC−MS experiments were performed on a Hewlett-Packard 6890 gas chromatograph fitted with a J&W Scientific DB-5MS column [30 m × 0.25 mm (internal diameter)] and a Micromass GCT Premiere detecting in the range of m/z 50−800 in EI^+ mode with scanning once a second with a scan time of 0.9 s. Injections were performed in split mode (split ratio of 5:1) at 50 °C. Chromatograms were begun with an oven temperature of 50 °C rising at 4 °C min^{-1} for 25 min (up to 150 °C) and then at 20 °C min^{-1} for 5 min (final temperature of 250 °C).

Crystallization and Structure Determination. Crystals of DCS were grown by the hanging drop vapor diffusion method. Briefly, a drop containing 5 μL of protein solution [10 mg/mL DCS, 20 mM Tris (pH 8.0), 2 mM $MgCl_2$, and 5 mM BME] and 5 μL of precipitant solution [100 mM Tris (pH 7.5), 200 mM Li_2SO_4, 15−17% polyethylene glycol (PEG) 4000, and 100 mM $BaCl_2 \cdot 2H_2O$] was suspended over a reservoir of 600 μL of precipitant solution. Crystals of DCS grew within 1−2 days with dimensions of 0.2 mm × 0.2 mm × 0.1 mm. Crystals were soaked in a precipitant solution containing 5 mM 10-fluorofarnesyl diphosphate (10F-FPP) for 16 h and were cryoprotected in a similar precipitant solution containing 5 mM 10F-FPP, 5 mM $MnCl_2$, and 25% glycerol prior to being flash-cooled in liquid nitrogen. Crystals diffracted X-rays to 2.4 Å resolution at the Advanced Photon Source (APS) (Argonne National Laboratory, Argonne, IL), NE-CAT beamline 24-ID-C, and belonged to space group $P2_13$ with two molecules in the asymmetric unit (solvent content of 52%) and the following unit cell parameters: $a = b = c = 158.20$ Å. Data were processed using HKL2000 (*31*). Initial phases were determined by molecular replacement using Phaser (*32*), with *Nicotiana tabacum* 5-epi-aristolochene synthase (Protein Data Bank entry 5EAT, 48% amino acid sequence identity) (*33*) less all metal ions, ligands, and solvent molecules, used as a search probe. Iterative cycles of refinement and model building were performed with CNS (*34*), O (*35*), and Coot (*36*) to improve the structure as monitored by R_{free}. Strict noncrystallographic symmetry (NCS) constraints were used during the initial stages of refinement and then relaxed into appropriately weighted restraints as indicated by R_{free} as refinement progressed. The inspection of electron density maps did not reveal the presence of 10F-FPP, which was present in the crystal soaking buffer. Atomic displacement parameters were refined using the default restraints employed in PHENIX (*37*). Refinement was completed using PHENIX (*37*), and PROCHECK (*38*) was used to validate the structural model. Atomic coordinates of solvent molecules, two glycerol molecules, and two BME molecules were added during the last stages of refinement, and a disulfide linkage was observed between C408 and C447. One residue, F458 in monomer B, was found to adopt a disallowed backbone conformation; this residue is located in a partially disordered loop between helices H and Hα-1 and is characterized by moderately weak electron density. Disordered segments were excluded from the final model. Data collection and refinement statistics are listed in Table 1.

To determine the structure of the complex with 2-fluorofarnesyl diphosphate (2F-FPP), crystals of unliganded DCS were gradually transferred to a stabilizing solution containing 100 mM Tris (pH 7.5), 200 mM Li_2SO_4, 17−19% PEG 4000, and 2 mM 2F-FPP and allowed to soak for 16 h. Crystals were slowly cryoprotected with a stabilizing solution containing 2 mM $MnCl_2$ and 25% glycerol and then flash-cooled with liquid nitrogen. Data were collected to 2.75 Å resolution at SER-CAT beamline 22-ID, at APS. Crystals were isomorphous with those of the unliganded enzyme. Data collection and refinement were performed as described for the structure determination of unliganded DCS. Atomic coordinates of solvent molecules and

Table 1: Data Collection and Refinement Statistics

	unliganded DCS	DCS−2F-FPP
resolution range (Å)	50.0−2.40	50−2.75
no. of reflections (measured/unique)	98790/51262	130161/34661
completeness (%) (overall/outer shell)	99.4/100.0	99.9/99.9
R_{merge}[a] (overall/outer shell)	0.099/0.460	0.083/0.487
$\langle I/\sigma \rangle$ (overall/outer shell)	19.8/4.7	13.0/3.2
no. of protein atoms[b]	8390	8402
no. of solvent atoms[b]	380	177
no. of metal ions[b]	0	6
no. of ligand atoms[b]	0	50
Refinement		
no. of reflections used in refinement (work/free)	51193/2040	34635/1708
R/R_{free}[c]	0.187/0.239	0.201/0.256
average B factor (Å^2)		
protein main chain atoms	54	66
protein side chain atoms	78	68
2F-FPP	−	84
Mg^{2+} ions	−	58
β-mercaptoethanol	78	72
glycerol	84	−
water molecules	58	58
root-mean-square deviation		
bonds (Å)	0.010	0.010
angles (deg)	1.2	1.3
dihedral angles (deg)	18.4	21.4
Ramachandran plot		
most favored (%)	91.8	90.1
additionally allowed (%)	7.2	8.9
generously allowed (%)	0.9	1.0
disallowed (%)	0.1	0

[a] $R_{merge} = \sum|I_j - \langle I_j \rangle| / \sum I_j$, where I_j is the observed intensity for reflection j and $\langle I_j \rangle$ is the average intensity calculated for reflection j from replicate data. [b] Per asymmetric unit. [c] $R = \sum||F_o| - |F_c|| / \sum|F_o|$, where R and R_{free} are calculated using the working and test reflection sets, respectively.

2F-FPP were added during the last stages of refinement. Data collection and refinement statistics are reported in Table 1.

RESULTS

Inhibition of DCS by 2F-FPP. Incubation of DCS with 2F-FPP does not lead to the generation of any detectable pentane-extractable products by GC−MS even after extended incubation times. When incubated with the enzyme and 10 μM FPP, 2F-FPP exhibits an IC_{50} value of approximately 30 μM. However, despite repeated attempts to determine its mode of inhibition, no consistent behavior in this regard could be determined (see the Supporting Information). Similar complexity in the inhibition pattern of terpene synthases by substrate analogues is also observed for limonene synthase and bornyl diphosphate synthase (*39*). Regardless, we conclude that 2F-FPP is sufficiently stable for X-ray crystallographic studies with DCS (vide infra).

Structure of Unliganded DCS. The crystal structure of DCS is only the second to be reported to date for a plant sesquiterpene cyclase; the first was that of tobacco 5-epi-aristolochene synthase (*33*). Since the structure of DCS determined from crystals soaked with 10F-FPP contains no bound ligand, this structure provides a view of the unliganded enzyme. The structures of the two DCS monomers in the asymmetric unit are essentially identical; the root-mean-square deviation (rmsd) of 499 Cα atoms between monomers A and B is 0.68 Å. The buried surface area between monomers A and B is 637 Å^2, which is too small to indicate a biologically relevant dimer. This is consistent with gel permeation chromatography experiments showing that DCS functions as a monomer in solution (*7*). The rmsds of 499 Cα atoms between DCS and 5-epi-aristolochene synthase (the search probe used in molecular replacement calculations) is 1.0 Å.

The C-terminal catalytic domain of DCS adopts the α-helical class I terpenoid synthase fold (Figure 2) first observed for avian farnesyl diphosphate synthase (*21*). This fold was subsequently observed in sesquiterpene cyclases such as pentalenene synthase (*40*), 5-epi-aristolochene synthase (*33*), and monoterpene cyclases such as bornyl diphosphate synthase (*41*); structure−function relationships in the greater family of terpenoid cyclases have been reviewed (*24*−*27*, *42*). Six α-helices frame the ~18 Å deep active site cleft, and helices D and H are on opposite walls of this cleft. Analysis of the crystal structure confirms that the first aspartate-rich motif (D^{307}DTYD^{311}) is located on the C-terminal end of helix D and the second aspartate-rich motif (D^{451}DVAE^{455}) is located at the C-terminal end of helix H. The noncatalytic N-terminal domain of DCS adopts an α-helical fold comparable to that of a class II terpenoid synthase, as first noted (*25*) for the N-terminal domain of 5-epi-aristolochene synthase (*33*).

In monomers A and B, the N-termini (M1−K24 and M1−P29, respectively) and loop segments K42−I44 and K42−D45, F460−D464 and F460−D464, and G530−T534 and Y533−V536, respectively, are disordered and excluded from the final model. Apart from the K42−I44 or K42−D45 segment, each of these disordered segments is adjacent to the active site in the C-terminal domain. In some but not all unliganded terpenoid cyclases, one or more disordered polypeptide segments flank the mouth of the active site but become ordered upon the binding of magnesium ions and substrate analogues or products. Such structural transitions lead to a closed active site conformation that sequesters the substrate and reactive carbocation intermediates from bulk solvent, as recently reviewed (*26*, *27*).

Structure of the DCS−2F-FPP Complex. The overall conformation of DCS in its complex with the substrate analogue inhibitor 2F-FPP and three metal ions is similar to that of unliganded DCS (Figure 2), with an rmsd of 0.28 Å for 514 Cα atoms between the structures of liganded and unliganded monomer A and an rms deviation of 0.50 Å for 494 Cα atoms between the structures of liganded and unliganded monomer B. The binding of 2F-FPP does not rigidify disordered polypeptide segments: the N-termini (M1−K24) and loop segments K42−I44, F460−D464, and G530−T534 remain disordered in each monomer. This contrasts with structural changes observed upon binding of ligands to fungal terpenoid cyclases, in which significant active site conformational changes result in active site closure with rmsds of ~1.5 Å for Cα atoms between liganded and unliganded structures (*19*, *43*). Intriguingly, overall conformational changes between liganded and unliganded catalytic domains of plant cyclases are somewhat smaller than those observed for fungal cyclases. For example, although significant local structural changes are triggered by ligand binding to the active site of bornyl diphosphate synthase, the rmsd of 306 Cα atoms in the catalytic domain is only 0.61 Å (*41*). Ligand binding to the active site of 5-epi-aristolochene synthase results in partial ordering of loop residues flanking the active site, but otherwise only minimal overall structural changes result to yield an rmsd of

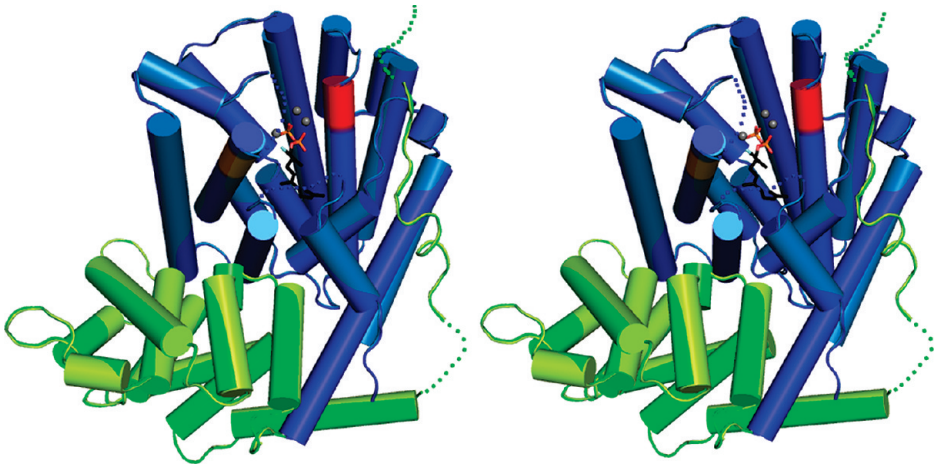

FIGURE 2: C-Terminal catalytic domain of DCS that adopts the α-helical class I terpenoid synthase fold (unliganded DCS, blue; 2F-FPP complex, light blue) and noncatalytic N-terminal domain that adopts an α-helical fold similar to that of a class II terpenoid synthase (unliganded DCS, green; 2F-FPP complex, light green). In the catalytic domain, the aspartate-rich $D^{307}DTYD^{311}$ metal binding motif on helix D is colored red and the second metal-binding motif, $D^{451}DVAE^{455}$, on helix H is colored orange. Disordered polypeptide segments are indicated by dotted lines. Putative Mg^{2+} ions are shown as small gray spheres. For 2F-FPP, atoms are color-coded as follows: black for C, red for O, orange for P, and light blue for F.

0.43 Å for 308 Cα atoms in the catalytic domain (*33*). Thus, it is possible that overall conformational changes triggered by ligand binding to the active sites of plant cyclases are somewhat attenuated in comparison with fungal cyclases, perhaps due to the presence of the additional N-terminal domain in the plant cyclases.

The binding of 2F-FPP to monomer A and monomer B is generally similar (Figure 3), and the overall rms deviation between monomer A and monomer B is 0.43 Å for 515 Cα atoms. The diphosphate group of 2F-FPP engages in few hydrogen bond interactions. In monomer A, the terminal diphosphate group of 2F-FPP accepts a hydrogen bond from R448, and the prenyl phosphoester oxygen donates a hydrogen bond to a water molecule that, in turn, accepts a hydrogen bond from R270. In monomer B, the corresponding interactions of the 2F-FPP diphosphate group are too long (3.5−3.6 Å) to be considered hydrogen bond interactions.

A Bijvoet difference Fourier map calculated with anomalous scattering data collected at $\lambda = 1.0$ Å does not reveal any peaks corresponding to bound Mn^{2+} or Ba^{2+} ions (data not shown; recall that DCS crystals were prepared in 100 mM $BaCl_2$ and cryoprotected in 2 mM $MnCl_2$). Although we cannot rule out low-occupancy binding of Mn^{2+} or Ba^{2+}, we conclude that the three electron density peaks observed in the active site adjacent to the aspartate-rich segments with peak heights of 12.5σ, 7.4σ, and 11.3σ correspond to putative $Mg^{2+}{}_A$, $Mg^{2+}{}_B$, and $Mg^{2+}{}_C$ ions, respectively. Importantly, the binding sites of these ions correspond to the binding sites of magnesium ions in other terpenoid synthases (Figure 4). Curiously, several residues that interact with the putative Mg^{2+} ions in DCS do so with separations that are too long to be considered inner sphere metal coordination interactions (average separation of 2.7 Å). While such interatomic separations are more consistent with hydrogen bond interactions than inner sphere metal coordination interactions (indeed, we considered that the potential metal binding sites could be occupied by water molecules instead of Mg^{2+} ions), we ultimately disfavored the interpretation of solvent molecules due to the electron density peak heights observed for the three putative Mg^{2+} ions. If these peaks correspond to Mg^{2+} ions, then perhaps their interactions become closer and stronger upon the transition from an "open" to a "closed" active site conformation.

Mutagenesis of the Aspartate-Rich Motifs. To further probe the role of the aspartate-rich $D^{307}DTYD^{311}$ motif on helix D that interacts with the putative $Mg^{2+}{}_A$ and $Mg^{2+}{}_C$ ions, the D307A, D308A, and D311A mutants have been produced and purified using a protocol similar to that used for the purification of wild-type DCS. All mutant proteins generate δ-cadinene as the sole product as determined by GC−MS (see the Supporting Information). For the cyclization of FPP by D308A DCS, $K_M = 43 \pm 16$ μM and $k_{cat} = 0.012 \pm 0.001$ s^{-1}. In comparison, the cyclization of FPP by wild-type DCS yields a K_M of 3.2 ± 0.5 μM and a k_{cat} of 0.010 ± 0.001 s^{-1}. However, it is not possible to determine steady-state kinetic parameters for catalysis by D307A DCS and D311A DCS because the rate of δ-cadinene production is so low that it is beyond the capacity of the kinetic assays to measure.

To probe the role of the second aspartate-rich motif ($D^{451}DVAE^{455}$) on helix H that interacts with the putative $Mg^{2+}{}_B$ ion, the D451A, D452A, and E455A mutants have been similarly produced and purified. While E455A DCS still generates δ-cadinene, it is not possible to determine steady-state kinetic parameters for catalysis due to the very low activity of this mutant. In contrast, the steady-state kinetic parameters for the cyclization of FPP by D451A DCS ($K_M = 2.4 \pm 0.3$ μM, and $k_{cat} = 0.043 \pm 0.001$ s^{-1}) and D452A DCS ($K_M = 3.1 \pm 1.2$ μM, and $k_{cat} = 0.014 \pm 0.001$ s^{-1}) are comparable to those measured for the wild-type enzyme.

DISCUSSION

DCS Contains a Unique Metal Binding Motif. Although DCS contains the aspartate-rich motif **D**DXX(**D**,**E**) (boldface residues coordinate metal ions) common to helix D of the terpenoid cyclases, it does not contain the NSE/DTE metal binding motif common to helix H of the terpenoid cyclases usually occurring as **D**DXX**T**XXX**E** in plant cyclases (*18*, *19*, *33*, *41*, *44*, *45*). Instead, DCS contains a second aspartate-rich sequence ($\mathbf{D}^{451}DVA\mathbf{E}^{455}$). Interestingly, the prenyltransferase farnesyl diphosphate synthase (FPPS) is an isoprenoid chain

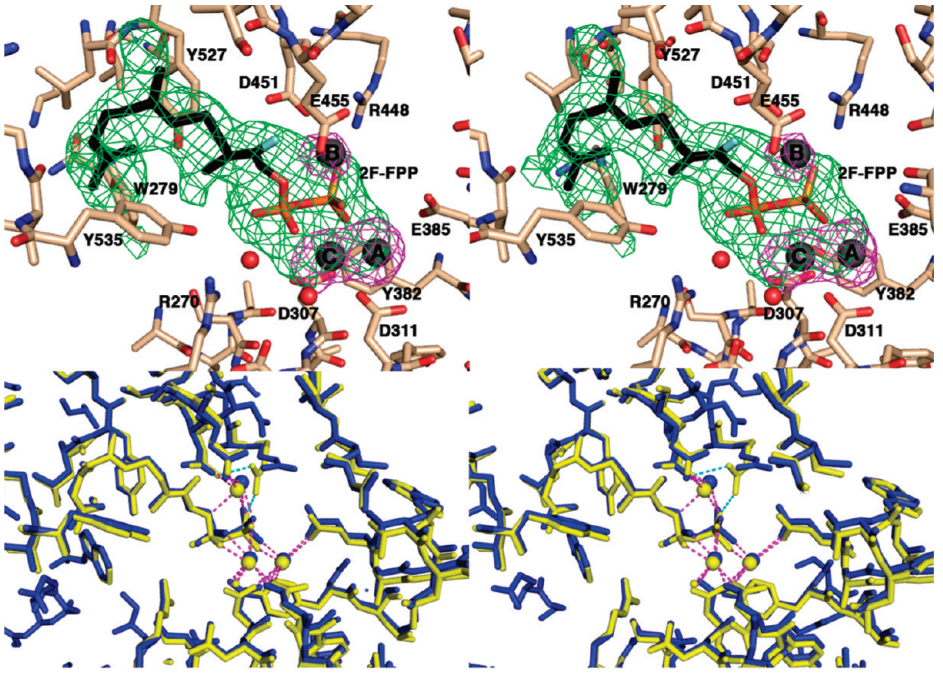

FIGURE 3: (a) Simulated annealing omit maps of 2F-FPP (green, contoured at 3.5σ) and putative Mg^{2+} ions (magenta, contoured at 4.0σ) in monomer A of the DCS−2F-FPP complex. Selected active site residues are indicated, and atoms are color-coded as follows: tan (DCS) or black (2F-FPP) for C, red for O, blue for N, orange for P, green for S, and light blue for F. Putative Mg^{2+} ions are depicted as gray spheres, and water molecules are depicted as red spheres. (b) Stereoview of the superposition of monomer A (yellow) and monomer B (blue) of the DCS−2F-FPP complex showing that isoprenoid binding is generally similar in both monomers. Dashed lines represent Mg^{2+} (magenta) and hydrogen bond (green) interactions.

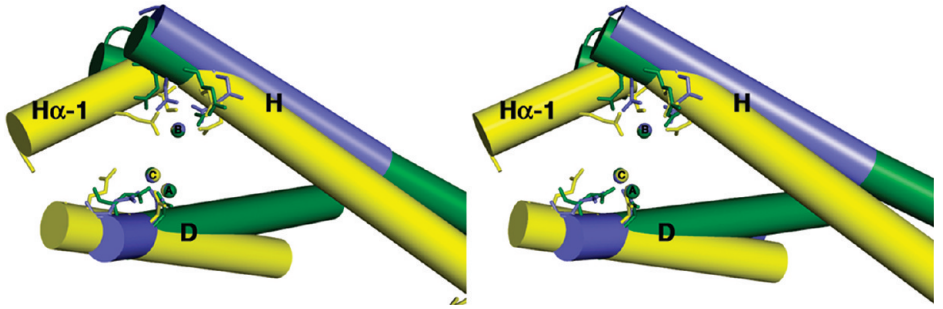

FIGURE 4: Superposition of helices D and H of *A. terreus* aristolochene synthase complexed with PP_i (yellow), *Escherichia coli* farnesyl diphosphate synthase complexed with isopentenyl diphosphate and dimethylallyl *S*-thiolodiphosphate (green), and DCS complexed with 2F-FPP (blue), based on the superposition of their trinuclear metal clusters. For the sake of clarity, only residues interacting with $Mg^{2+}{}_A$, $Mg^{2+}{}_B$, and $Mg^{2+}{}_C$ are shown on helices D, H, and Hα-1. The constellation of three magnesium ions is identical regardless of whether $Mg^{2+}{}_B$ is chelated by an aspartate-rich motif or the NSE/DTE motif, and regardless of whether the enzyme catalyzes an isoprenoid chain elongation reaction or a cyclization reaction. Coordination of $Mg^{2+}{}_B$ by an NSE/DTE motif requires the additional helix Hα-1.

elongation enzyme rather than a cyclase, and this enzyme contains two conserved aspartate-rich DDXXD metal binding motifs. Peters has shown that the serine/threonine $Mg^{2+}{}_B$ ligand in the NSE/DTE motif of certain plant cyclases is occasionally substituted with glycine, potentially allowing for an additional water molecule in the $Mg^{2+}{}_B$ coordination polyhedron (*20*). Thus, the NSE/DTE motif for $Mg^{2+}{}_B$ binding is not an absolutely universal signature sequence distinguishing a terpenoid cyclase from the greater family of terpenoid synthases such as FPPS. Curiously, FPPS is known to generate low levels of cyclic sesquiterpenoids (*46*), so the functional distinction between a cyclase and a chain elongation enzyme is likely to reside in the active site contour, i.e., the overall template for the reaction, and the carbon−carbon bond forming reactions permitted or prevented by this template.

Interestingly, mutations to the aspartate-rich motifs D^{307}-DTYD^{311} and D^{451}DVAE^{455} of DCS, where each aspartate residue is individually replaced with alanine, do not completely obliterate catalytic activity. However, the D307A, D311A, and E455A substitutions severely compromise activity, which is consistent with the critical role of these residues in orienting the trinuclear magnesium cluster (Figure 3). In contrast, the D308A, D451A, and D452A substitutions result in essentially unchanged turnover numbers. It is curious that the D451A substitution in the second aspartate-rich motif does not impact catalysis, since this residue interacts with the putative $Mg^{2+}{}_B$ ion (Figure 3) and the corresponding aspartate does likewise in FPPS (*22*). Regardless, mutagenesis of E455 in DCS shows that the third carboxylate residue in the second aspartate-rich motif plays a significant role in metal binding and catalysis, whereas the

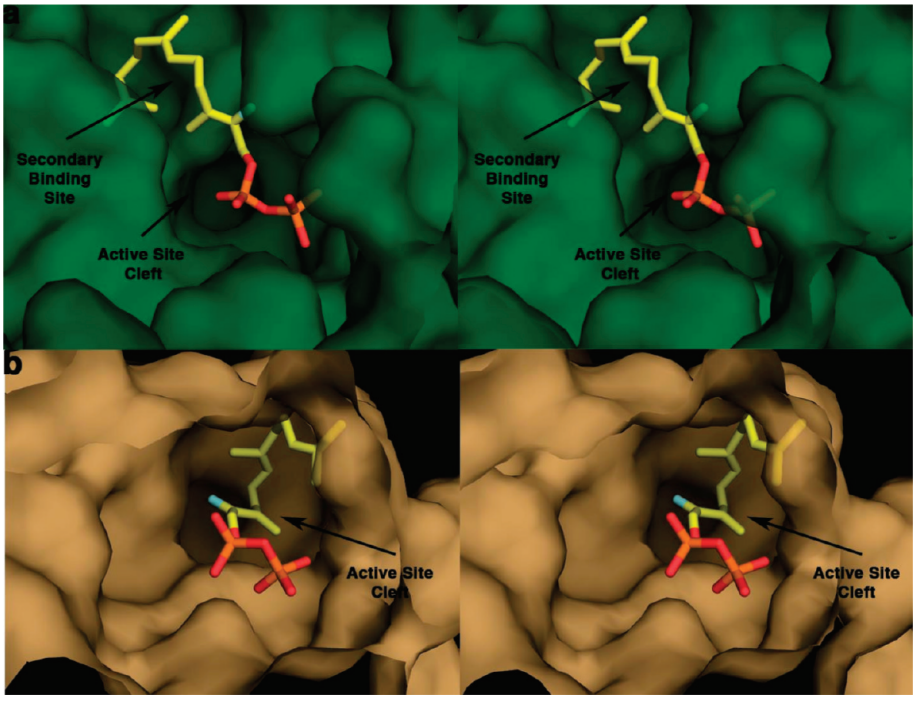

FIGURE 5: Stereoviews of active site contours of DCS (a) and *A. terreus* aristolochene synthase (b) looking into the ~18 Å deep active site clefts. The isoprenoid moiety of the substrate analogue 2F-FPP binds in a secondary cleft adjacent to the main active site cleft of DCS. In contrast, the isoprenoid moiety of 2F-FPP binds in the main active site cleft of aristolochene synthase (*28*).

corresponding residue in FPPS does not interact with $Mg^{2+}{}_B$. Therefore, subtle differences in metal binding interactions by conserved motifs can distinguish one terpenoid synthase from another.

Notably, while the K_M for D308A DCS is increased 13-fold, it is largely unchanged for D451A DCS and D452A DCS. Mutagenesis experiments with other terpenoid synthases show that the second aspartate of the aspartate-rich motif can have a variable influence on catalytic activity (*47*−*50*). Presumably, such effects depend on the intramolecular interactions of the second aspartate residue in the enzyme−substrate complex. For example, the second aspartate residue in the aspartate-rich motifs of the fungal cyclases trichodiene synthase and aristolochene synthase engages in a salt link with an arginine residue to stabilize closed active site conformations (*19*, *43*). However, the side chain of D308 in DCS does not engage in hydrogen bond interactions in the crystal structures of unliganded DCS and its 2F-FPP complex.

When the trinuclear metal clusters of DCS, *A. terreus* aristolochene synthase (ATAS) (*43*), and *E. coli* FPPS (*22*) are compared, interesting similarities in metal ion interactions are observed despite the divergent evolution of the $Mg^{2+}{}_B$ binding motif (Figure 4). In the DCS−$Mg^{2+}{}_3$−2F-FPP complex, $Mg^{2+}{}_B$ interacts with D451, E455, and one oxygen of the 2F-FPP diphosphate group. In the ATAS−$Mg^{2+}{}_3$−PP_i complex, $Mg^{2+}{}_B$ is coordinated by E227, N219, S223, and two oxygen atoms of PP_i. Similarly, in the FPPS−$Mg^{2+}{}_3$−isopentenyl diphosphate−dimethylallyl-*S*-thiolodiphosphate complex, $Mg^{2+}{}_B$ is coordinated by D244, two oxygen atoms of the isopentenyl diphosphate group, and three water molecules. Comparison of these structures reveals that when $Mg^{2+}{}_B$ is coordinated by a DDXXD/E motif, the metal binding residues are contained on a single, unbent helix H; when $Mg^{2+}{}_B$ is coordinated by an NSE/DTE motif, a bend or an additional short helix (helix Hα-1) containing the serine/threonine and glutamate residues of the NSE/DTE motif is found at the C-terminal end of helix H. This conclusion also holds true for the structures of other terpenoid synthases determined in the presence of metal ions (*19*, *33*, *41*, *43*, *44*).

Concluding Remarks. On the basis of the conformation of 2F-FPP in the active site and the proposed catalytic mechanism for DCS (Figure 1), the C10 and C1 atoms are too far apart (> 6 Å) for the initial cyclization reaction to occur. This is a likely consequence of 2F-FPP binding in what appears to be a secondary isoprenoid binding site adjacent to the active site cleft of DCS (Figure 5). It is not clear whether this secondary isoprenoid binding site is important for catalysis. However, 2F-FPP appears to have a complex mode of inhibition (see Figure S10 of the Supporting Information), which could be consistent with the alternative mode of binding observed in the crystal structure.

Intermolecular interactions observed in the DCS active site nevertheless yield insight into metal coordination that is relevant to our understanding of catalysis. Although DCS contains a different motif for $Mg^{2+}{}_B$ coordination, this cyclase shares a similar constellation of three Mg^{2+} ions for activating the substrate diphosphate group with other terpenoid cyclases such as 5-epi-aristolochene synthase (*33*), trichodiene synthase (*19*), limonene synthase (*44*), cineole synthase (*45*), aristolochene synthase (*43*, *51*), and bornyl diphosphate synthase (*41*). Accordingly, despite the divergent evolution of terpenoid synthases in all forms of life, the chemical strategy for the activation of isoprenoid diphosphate substrates with three metal ions is conserved and is also shared with isoprenoid elongation enzymes such as FPPS (*22*) and geranylgeranyl diphosphate synthase (*52*). This study suggests that an aspartate-rich **D**DXX(X)**D/E** motif on helix H signals a single helix bearing potential $Mg^{2+}{}_B$ ligands (boldface) and an NSE/DTE motif (**N**,**D**)D(L,I,V)X(**S**,**T**)XXX**E** signals a bend or an additional short helix (helix Hα-1) at the C-terminal end of helix H such that the first $Mg^{2+}{}_B$ ligand in this motif (**N**,**D**) is on helix H, and the remaining $Mg^{2+}{}_B$ ligands

(**S**,**T**)XXX**E** are on the bend or on helix Hα-1 (Figure 4). We conclude that the distinction between an isoprenoid chain elongation enzyme and a cyclase is not necessarily rooted in the specific motifs for metal binding but instead in the three-dimensional contour of the active site and the carbon−carbon bond forming reactions permitted or prevented by this template for catalysis.

ACKNOWLEDGMENT

We thank Dr. Xiao-Ya Chen (Institute of Plant Physiology and Ecology, Shanghai Institutes for Biological Sciences, Shanghai, China) for plasmid pXC1 and Dr. Susan E. Taylor for help with the early parts of this project. Data were collected on Southeast Regional Collaborative Access Team (SER-CAT) beamline 22-ID at the Advanced Photon Source, Argonne National Laboratory. Supporting Institutions may be found at www.ser-cat.org/members.html. Data were also collected at Northeastern Collaborative Access Team (NE-CAT) beamline 24-ID-C (supported by National Institutes of Health Grant RR15301) at the Advanced Photon Source, Argonne National Laboratory. Use of the Advanced Photon Source was supported by the U.S. Department of Energy, Office of Science, Office of Basic Energy Sciences, under Contracts W-31-109-Eng-38 and DE-AC02-06CH11357.

SUPPORTING INFORMATION AVAILABLE

Detailed materials and methods for the synthesis of 10-fluorofarnesyl diphosphate, gas chromatography and mass spectroscopic analysis of cyclization product generated by wild-type and mutant DCS enzymes, and enzyme kinetic data. This material is available free of charge via the Internet at http://pubs.acs.org.

REFERENCES

(1) Bell, A. A., Stipanovic, R. D., Howell, C. R., and Fryxell, P. A. (1975) Antimicrobial terpenoids of *Gossypium*: Hemigossypol, 6-methoxyhemigossypol and 6-deoxyhemigossypol. *Phytochemistry 14*, 225–231.

(2) Bell, A. A. (1986) Physiology of secondary products. In Cotton Physiology (Mauney, J. R., and McStewart, J., Eds.) pp 597−622, The Cotton Foundation, Memphis, TN.

(3) Chappell, J. (1995) The biochemistry and molecular biology of isoprenoid metabolism. *Plant Physiol. 107*, 1–6.

(4) Benedict, C. R., Alchanati, I., Harvey, P. J., Liu, J., Stipanovic, R. D., and Bell, A. A. (1995) The enzymatic formation of δ-cadinene from farnesyl diphosphate in extracts of cotton. *Phytochemistry 39*, 327–331.

(5) Chen, X. Y., Chen, Y., Heinstein, P., and Davisson, V. J. (1995) Cloning, expression, and characterization of (+)-δ-cadinene synthase: A catalyst for cotton phytoalexin biosynthesis. *Arch. Biochem. Biophys. 324*, 255–266.

(6) Davis, G. D., and Essenberg, M. (1995) (+)-δ-Cadinene is a product of sesquiterpene cyclase activity in cotton. *Phytochemistry 39*, 553–567.

(7) Davis, E. M., Tsuji, J., Davis, G. D., Pierce, M. L., and Essenberg, M. (1996) Purification of (+)-δ-cadinene synthase, a sesquiterpene cyclase from bacteria-inoculated cotton foliar tissue. *Phytochemistry 41*, 1047–1055.

(8) Coutinho, E. M. (2002) Gossypol: A contraceptive for men. *Contraception 65*, 259–263.

(9) Cui, G. H., Xu, Z. L., Yang, Z. J., Xu, Y. Y., and Xue, S. P. (2004) A combined regimen of gossypol plus methyltestosterone and ethinylestradiol as a contraceptive induces germ cell apoptosis and expression of its related genes in rats. *Contraception 70*, 335–342.

(10) Band, V., Hoffer, A. P., Band, H., Rhinehardt, A. E., Knapp, R. C., Matlin, S. A., and Anderson, D. J. (1989) Antiproliferative effect of gossypol and its optical isomers on human reproductive cancer cell lines. *Gynecol. Oncol. 32*, 273–277.

(11) Balci, A., Sahin, F. I., and Ekmekci, A. (1999) Gossypol induced apoptosis in the human promyelocytic leukemia cell line HL 60. *Tohoku J. Exp. Med. 189*, 51–57.

(12) Wang, X., Wang, J., Wong, S. C., Chow, L. S., Nicholls, J. M., Wong, Y. C., Liu, Y., Kwong, D. L., Sham, J. S., and Tsa, S. W. (2000) Cytotoxic effect of gossypol on colon carcinoma cells. *Life Sci. 67*, 2663–2671.

(13) Zhang, M., Liu, H., Guo, R., Ling, Y., Wu, X., Li, B., Roller, P. P., Wang, S., and Yang, D. (2003) Molecular mechanism of gossypol-induced cell growth inhibition and cell death of HT-29 human colon carcinoma cells. *Biochem. Pharmacol. 66*, 93–103.

(14) Benedict, C. R., Lu, J.-L., Pettigrew, D. W., Liu, J., Stipanovic, R. D., and Williams, H. J. (2001) The cyclization of farnesyl diphosphate and nerolidyl diphosphate by a purified recombinant δ-cadinene synthase. *Plant Physiol. 125*, 1754–1765.

(15) Yoshikuni, Y., Martin, V. J. J., Ferrin, T. E., and Keasling, J. D. (2006) Engineering cotton (+)-δ-cadinene synthase to an altered function: Germacrene D-4-ol synthase. *Chem. Biol. 13*, 91–98.

(16) Lodewyk, M. W., Gutta, P., and Tantillo, D. J. (2008) Computational studies on biosynthetic carbocation rearrangements leading to sativene, cyclosativene, α-ylangene, and β-ylangene. *J. Org. Chem. 73*, 6570–6579.

(17) Steele, C. L., Crock, J., Bohlmann, J., and Croteau, R. (1998) Sesquiterpene synthases from grand fir (*Abies grandis*). Comparison of constitutive and wound-induced activities, and cDNA isolation, characterization, and bacterial expression of δ-selinene synthase and γ-humulene synthase. *J. Biol. Chem. 273*, 2078–2089.

(18) Cane, D. E., and Kang, I. (2000) Aristolochene synthase: Purification, molecular cloning, high-level expression in *Escherichia coli*, and characterization of the *Aspergillus terreus* cyclase. *Arch. Biochem. Biophys. 376*, 354–364.

(19) Rynkiewicz, M. J., Cane, D. E., and Christianson, D. W. (2001) Structure of trichodiene synthase from *Fusarium sporotrichioides* provides mechanistic inferences on the terpene cyclization cascade. *Proc. Natl. Acad. Sci. U.S.A. 98*, 13543–13548.

(20) Zhou, K., and Peters, R. J. (2009) Investigating the conservation pattern of a putative second terpene synthase divalent metal binding motif in plants. *Phytochemistry 70*, 366–369.

(21) Tarshis, L. C., Yan, M., Poulter, C. D., and Sacchettini, J. C. (1994) Crystal structure of recombinant farnesyl diphosphate synthase at 2.6 Å resolution. *Biochemistry 33*, 10871–10877.

(22) Hosfield, D. J., Zhang, Y., Dougan, D. R., Broun, A., Tari, L. W., Swanson, R. V., and Finn, J. (2004) Structural basis for bisphosphonate-mediated inhibition of isoprenoid biosynthesis. *J. Biol. Chem. 279*, 8526–8529.

(23) Kellogg, B. A., and Poulter, C. D. (1997) Chain elongation in the isoprenoid biosynthetic pathway. *Curr. Opin. Chem. Biol. 1*, 570–578.

(24) Lesburg, C. A., Caruthers, J. M., Paschall, C. M., and Christianson, D. W. (1998) Managing and manipulating carbocations in biology: Terpenoid cyclase structure and mechanism. *Curr. Opin. Struct. Biol. 8*, 695–703.

(25) Wendt, K. U., and Schulz, G. E. (1998) Isoprenoid biosynthesis: manifold chemistry catalyzed by similar enzymes. *Structure 6*, 127–133.

(26) Christianson, D. W. (2006) Structural biology and chemistry of the terpenoid cyclases. *Chem. Rev. 106*, 3412–3442.

(27) Christianson, D. W. (2008) Unearthing the roots of the terpenome. *Curr. Opin. Chem. Biol. 12*, 141–150.

(28) Shishova, E. Y., Yu, F., Miller, D. J., Faraldos, J. A., Zhao, Y., Coates, R. M., Allemann, R. K., Cane, D. E., and Christianson, D. W. (2008) X-ray crystallographic studies of substrate binding to aristolochene synthase suggest a metal ion binding sequence for catalysis. *J. Biol. Chem. 283*, 15431–15439.

(29) Miller, D. J., Yu, F., and Allemann, R. K. (2007) Aristolochene synthase-catalyzed cyclization of 2-fluorofarnesyl-diphosphate to 2-fluorogermacrene A. *ChemBioChem 8*, 1819–1825.

(30) Calvert, M. J., Ashton, P. R., and Allemann, R. K. (2002) Germacrene A is a product of the aristolochene synthase-mediated conversion of farnesylpyrophosphate to aristolochene. *J. Am. Chem. Soc. 124*, 11636–11641.

(31) Otwinowski, Z., and Minor, W. (1997) Processing of X-ray diffraction data collected in oscillation mode. *Methods Enzymol. 276*, 307–326.

(32) McCoy, A. J., Grosse-Kunstleve, R. W., Adams, P. D., Winn, M. D., Storoni, L. C., and Read, R. J. (2007) Phaser crystallographic software. *J. Appl. Crystallogr. 40*, 658–674.

(33) Starks, C. M., Back, K., Chappell, J., and Noel, J. P. (1997) Structural basis for cyclic terpene biosynthesis by tobacco 5-epi-aristolochene synthase. *Science 277*, 1815–1820.

(34) Brunger, A. T., Adams, P. D., Clore, G. M., DeLano, W. L., Gros, P., Grosse-Kunstleve, R. W., Jiang, J.-S., Kuszewski, J., Nilges, M., Pannu, N. S., Read, R. J., Rice, L. M., Simonson, T., and Warren, G. L. (1998) Crystallography & NMR system: A new software suite for macromolecular structure determination. *Acta Crystallogr. D54*, 905–921.
(35) Jones, T. A., Zou, J.-Y., Cowan, S. W., and Kjeldgaard, M. (1991) Improved methods for building protein models in electron density maps and the location of errors in these models. *Acta Crystallogr. A47*, 110–119.
(36) Emsley, P., and Cowtan, K. (2004) Coot: Model-building tools for molecular graphics. *Acta Crystallogr. D60*, 2126–2132.
(37) Afonine, P. V., Grosse-Kunstleve, R. W., and Adams, P. D. (2005) The Phenix refinement framework. CCP4 Newsletter 42 , contribution 8.
(38) Laskowski, R. A., MacArthur, M. W., Moss, D. S., and Thornton, J. M. (1993) PROCHECK: A program to check the stereochemical quality of protein structures. *J. Appl. Crystallogr. 26*, 283–291.
(39) Karp, F., Zhao, Y., Santhamma, B., Assink, B., Coates, R. M., and Croteau, R. B. (2007) Inhibition of monoterpene cyclases by inert analogues of geranyl diphosphate and linalyl diphosphate. *Arch. Biochem. Biophys. 468*, 140–146.
(40) Lesburg, C. A., Zhai, G., Cane, D. E., and Christianson, D. W. (1997) Crystal structure of pentalenene synthase: Mechanistic insights on terpenoid cyclization reactions in biology. *Science 277*, 1820–1824.
(41) Whittington, D. A., Wise, M. L., Urbansky, M., Coates, R. M., Croteau, R. B., and Christianson, D. W. (2002) Bornyl diphosphate synthase: Structure and strategy for carbocation manipulation by a terpenoid cyclase. *Proc. Natl. Acad. Sci. U.S.A. 99*, 15375–15380.
(42) Allemann, R. K. (2008) Chemical wizardry? The generation of chemical diversity in terpenoid biosynthesis. *Pure Appl. Chem. 80*, 1773–1780.
(43) Shishova, E. Y., Di Costanzo, L., Cane, D. E., and Christianson, D. W. (2007) X-ray crystal structure of aristolochene synthase from *Aspergillus terreus* and evolution of templates for the cyclization of farnesyl diphosphate. *Biochemistry 46*, 1941–1951.
(44) Hyatt, D. C., Youn, B., Zhao, Y., Santhamma, B., Coates, R. M., Croteau, R. B., and Kang, C. (2007) Structure of limonene synthase, a simple model for terpenoid cyclase catalysis. *Proc. Natl. Acad. Sci. U.S.A. 104*, 5360–5365.
(45) Kampranis, S. C., Ioannidis, D., Purvis, A., Mahrez, W., Ninga, E., Katerelos, N. A., Anssour, S., Dunwell, J. M., Degenhart, J., Makris, A. M., Goodenough, P. W., and Johnson, C. B. (2007) Rational conversion of substrate and product specificity in a *Salvia* monoterpene synthase: Structural insights into the evolution of terpene synthase function. *Plant Cell 19*, 1994–2005.
(46) Saito, A., and Rilling, H. C. (1980) The formation of cyclic sesquiterpenes from farnesyl pyrophosphate by prenyltransferase. *Arch. Biochem. Biophys. 208*, 508–511.
(47) Felicetti, B., and Cane, D. (2004) Aristolochene synthase: Mechanistic analysis of active site residues by site-directed mutagenesis. *J. Am. Chem. Soc. 126*, 7212–7221.
(48) Song, L., and Poulter, C. D. (1994) Yeast farnesyl-diphosphate synthase: Site-directed mutagenesis of residues in highly conserved prenyltransferase domains I and II. *Proc. Natl. Acad. Sci. U.S.A. 91*, 3044–3048.
(49) Cane, D. E., Xue, Q., and Fitzsimons, B. C. (1996) Trichodiene synthase. Probing the role of the highly conserved aspartate-rich region by site-directed mutagenesis. *Biochemistry 35*, 12369–12376.
(50) Seemann, M., Zhai, G., de Kraker, J.-W., Paschall, C. M., Christianson, D. W., and Cane, D. E. (2002) Pentalenene synthase. Analysis of active site residues by site-directed mutagenesis. *J. Am. Chem. Soc. 124*, 7681–7689.
(51) Caruthers, J. M., Kang, I., Rynkiewicz, M. J., Cane, D. E., and Christianson, D. W. (2000) Crystal structure determination of aristolochene synthase from the blue cheese mold *Penicillium roqueforti*. *J. Biol. Chem. 275*, 25533–25539.
(52) Kloer, D. P., Welsch, R., Beyer, P., and Schulz, G. E. (2006) Structure and reaction geometry of geranylgeranyl diphosphate synthase from *Sinapis alba*. *Biochemistry 45*, 15197–15204.